

Inelastic-neutron-scattering study of methyl tunneling and the quantum sine-Gordon breather in isotopic mixtures of 4-methyl-pyridine at low temperature

F. Fillaux

*Laboratoire de Spectrochimie Infrarouge et Raman, Centre National de la Recherche Scientifique,
2 rue Henri-Dunant, 94320 Thiais, France*

C. J. Carlile

ISIS Pulsed Neutron Facility, Rutherford Appleton Laboratory, Chilton, Didcot, Oxfordshire OX11 0QX, United Kingdom

(Received 20 March 1990)

The inelastic-neutron-scattering spectra in the 500- μeV region of a series of mixtures of totally hydrogenated and totally deuterated 4-methyl-pyridine molecules (4MP- h_7 and 4MP- d_7 , respectively) with relative concentrations in 4MP- h_7 of 100, 85, 65, 50, 26, 20, and 5% are presented at various temperatures: 2.5, 4.5, 6.5, 8.5, 11 and 15 K. In pure 4MP- h_7 at 2.5 K, the spectrum shows three partially resolved bands at 468, 510, and 535 μeV . These frequencies are unaffected by temperature up to 15 K where the bands become rather weak. At 2.5 K, the main peak shows a continuous frequency shift with increasing concentration in 4MP- d_7 down to 360 μeV (5% 4MP- h_7) indicating collective motions of the methyl groups. This frequency shift is very sensitive to temperature and vanishes above 10 K. These unusual aspects of the methyl-group dynamics are quantitatively represented by the quantum sine-Gordon equation describing a one-dimensional infinite chain of coupled methyl groups. Accordingly, the weak side bands at 468 and 535 μeV are assigned to in-phase and out-of-phase tunneling transitions, respectively. The main peak at 510 μeV in pure 4MP- h_7 is due to the excitation of the first quantized traveling state of the breather mode. Isotopic dilution effects are understood in terms of breathers trapped in clusters of 4MP- h_7 molecules surrounded by 4MP- d_7 molecules which act as reflective walls. Temperature effects are due to the thermal excitation of breather-roton states in relationship with the zero-point energy difference for 4MP- h_7 and 4MP- d_7 clusters. Finally, some previous spectroscopic data are reconsidered on the basis of the quantum sine-Gordon theory.

INTRODUCTION

This paper concerns the torsional dynamics of the methyl groups in solid 4-methyl-pyridine ($\text{C}_6\text{H}_7\text{N}$, and otherwise known as γ picoline) (Fig. 1) at very low temperatures. Since the methyl group is linked to an aromatic ring, the potential barrier for internal rotation is extremely low for the isolated molecule^{1,2} and remains exceptionally small even in the crystalline state.³⁻¹⁰ Although this compound has been investigated using several different techniques [NMR,^{3,4} inelastic neutron scattering (INS),^{5,7,8} NQR,^{11,12} x-ray and neutron diffraction,^{13,14} infrared and Raman spectroscopy^{9,10}], the potential function governing the methyl torsion in the crystalline state is still a subject of discussion. The earliest studies of methyl tunneling using high-resolution INS (Ref. 5) revealed a strong transition at 4.19 cm^{-1} (520 μeV) and weaker features at 11.37 cm^{-1} (1.41 meV) and 15.48 cm^{-1} (1.92 meV), which were interpreted in terms of a sixfold potential with a barrier height less than 100 cm^{-1} (12.5 meV). The three bands were assigned to the $0 \rightarrow 1$, $1 \rightarrow 2$, and $0 \rightarrow 2$ transitions, respectively. The frequency ratio of approximately 5 ($\tau_{\text{CH}_3}/\tau_{\text{CD}_3}$) as measured by INS (Ref. 8) is consistent with tunneling in a periodic potential with either threefold or sixfold symmetry. Raman spectra at low temperature, on the other hand, sug-

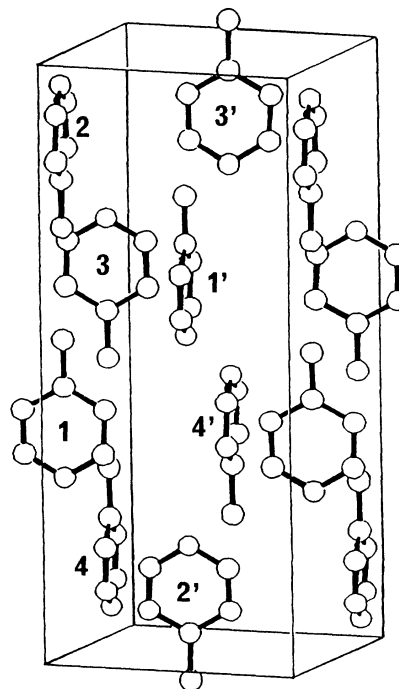


FIG. 1. Crystal structure of 4-methyl-pyridine at 4 K after Ref. 6.

gest very peculiar dynamics for the methyl rotation.^{9,10} Several transitions are identified unambiguously at low temperature. Surprisingly, frequencies are not consistent with a periodic barrier and correspond better to a non-periodic potential. This suggests a collective nature to the motion of the methyl groups.

New experimental data on 4MP at low temperature obtained with the IRIS spectrometer (ISIS pulsed neutron facility, Rutherford Appleton Laboratory, Chilton, United Kingdom) with a better resolution than in previous measurements⁸ are presented in this paper. Several components were resolved in the 4 cm^{-1} ($500 \mu\text{eV}$) region that had not been seen previously. In order to decide whether these components are due to intermolecular and/or intramolecular effects the spectra of a series of mixtures of totally hydrogenated (4MP- h_7) and totally deuterated (4MP- d_7) compounds were obtained in the $0\text{--}8 \text{ cm}^{-1}$ ($0\text{--}1 \text{ meV}$) region. The main band in the 4MP- h_7 spectrum showed a continuous frequency shift with increasing concentration of deuterated molecules, which confirms the existence of collective motions for the methyl groups. We are not aware of any similar effect having been observed previously for methyl rotation and we propose a totally new interpretation in terms of "breather" modes within the framework of the quantum sine-Gordon theory.

Experimental data for pure 4MP- h_7 , pure 4MP- d_7 , and various mixtures of h_7 and d_7 compounds between 2 and 15 K are presented in Sec. I of this paper. It is shown that they do not agree with the theoretical models already proposed for methyl tunneling. In Sec. II of the paper the classical and quantum sine-Gordon theories are applied to one-dimensional (1D) infinite chains of coupled methyl groups and the spectra of the quantum pseudoparticles (soliton, antisoliton, and breather) are characterized. In Sec. III, the INS spectra of 4MP- h_7 and 4MP- d_7 are interpreted in terms of traveling breathers in the crystal. In Sec. IV the frequency shifts observed in isotopic mixtures of h_7 and d_7 4MP at various temperatures are discussed in terms of breather dynamics in boxes of different sizes corresponding to hydrogenated and deuterated clusters. Finally, a general discussion reconsiders previous experimental data on the basis of possible breather and soliton dynamics and statistics.

I. EXPERIMENTAL DATA AND SPECTRA

A. Experimental

The deuterated compound (4-methyl-pyridine- d_7) was prepared by four exchanges with D_2O for 48 h in the presence of activated Raney nickel, followed by one exchange with D_2O in the presence of Adams platinum for 70 h at 125°C . NMR shows a total deuteration degree of 99.1% for the methyl group, 98.5% at the α position, and 99.3% at the β position.

The neutron-scattering experiments were carried out on the IRIS time of flight spectrometer¹⁵ at the ISIS pulsed neutron facility. IRIS is an inverted geometry inelastic neutron spectrometer that uses a long incident flight path and an array of pyrolytic graphite analyzers

close to back scattering to define both the incident and scattered neutron energies with high precision. The elastic resolution of the spectrometer is $15 \mu\text{eV}$ and the energy-transfer range available with good resolution is quite large. The low final energy of the crystal analyzers (1.82 meV) means that the spectrometer is particularly well suited for neutron energy-loss spectroscopy from cold samples.

Liquid mixtures of 4MP- h_7 and 4MP- d_7 at room temperature were introduced into aluminum cans about $40 \times 40 \times e \text{ mm}^3$ with $e=0.6, 0.6, 1.0, 1.0, 1.0, 2.0,$ and 5.0 mm for 100, 85, 65, 50, 26, 20, and 5 % concentrations in 4MP- h_7 , respectively. Cans were loaded into a liquid-helium cryostat and the temperature as controlled to $\pm 0.5 \text{ K}$.

B. Crystal structure

The crystal structure of 4-methyl-pyridine at 4 K (Fig. 1) (Ref. 16) is tetragonal, $I4_1/a$ (C_{4h}^6) with four molecules in the primitive cell. The site symmetry is C_2 and the methyl groups are disordered. The dominant dipole-dipole interaction leads to an antiparallel ordering of the molecules with respect to the c axis. The shortest intermolecular distance, a methyl-methyl contact parallel to the c axis of 3.462 \AA , is significantly shorter than the sum of van der Waals radii for two methyl groups of about 4 \AA (see for instance molecules labeled 1 and 2 or 3 and 4 on Fig. 1). Ohms and co-workers¹⁴ state that this short $\text{CH}_3\text{-CH}_3$ distance is only possible if there exists a strong correlation between the mutual orientation of adjacent methyl groups of different molecules. They should be twisted by 60° with respect to each other and perform combined hindered rotations.

Beside these close contact pairs, the next shortest methyl-methyl distances ($\sim 4.0 \text{ \AA}$ for molecules labeled 1 and 3 or 4 and 4' on Fig. 1) occur perpendicular to the c crystal axis. They form two different sets of equivalent infinite chains made of equidistant methyl groups with their mean directions parallel to the a or b crystal axis, respectively. a and b chains are not located in the same (a, b) planes. The other methyl-methyl distances are larger than 6 \AA .

High resolution neutron powder diffraction data ($\Delta d/d \sim 4.10^{-4}$) have been obtained recently for 4MP- h_7 and 4MP- d_7 at 4 K.¹⁶ On account of thermal contraction the cell dimensions are about 1% smaller than those determined at 120 K .¹⁴ The crystal structure is unaffected by temperature or deuteration. This confirms that the phase transition near 100 K observed by Raman¹⁰ is mainly due to some modification of the methyl-group dynamics. The monoclinic structure at 90 K proposed by Biswas¹³ is not confirmed.

C. Experimental data

The INS spectra of six different isotopic mixtures of 4MP- h_7 and 4MP- d_7 , at 2.5 K are presented in Figs. 2 and 3. In Figs. 4 and 5 are plotted the frequencies of the band maxima. Three major factors emerge from these data.

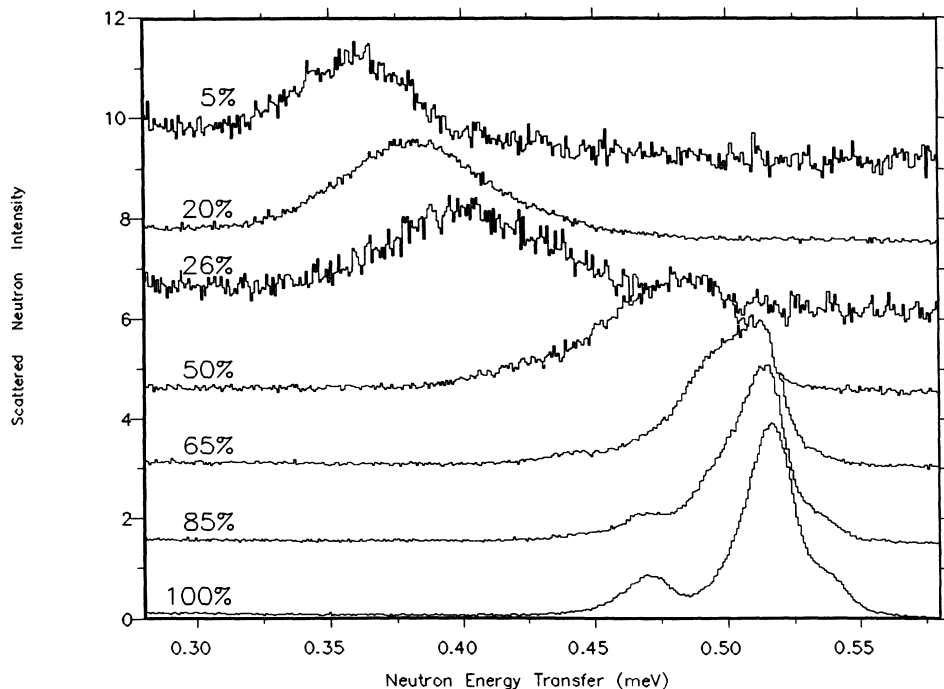


FIG. 2. Inelastic neutron scattering spectra at 2.5 K of isotopic mixtures of 4-methyl-pyridine and its perdeuterated derivative.

(i) There are clearly three components in the pure 4MP- h_7 crystal at 2.5 K. Further decomposition of the main peak into two components was proposed previously¹⁷ on the basis of band shape analysis and maximum entropy analysis with a Gaussian resolution function. How-

ever, a more rigorous analysis, including the true resolution function of the spectrometer, which is rather asymmetric, does not confirm this conclusion and throws doubt on the existence of the fourth component. At the present stage of the spectrometer development, systemat-

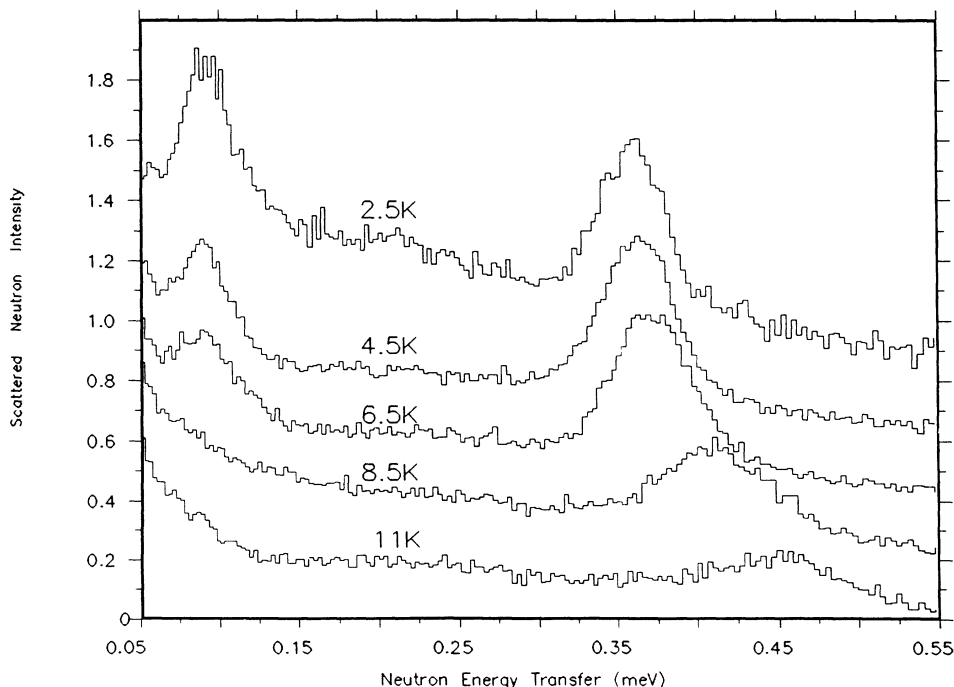


FIG. 3. Inelastic neutron scattering spectra at various temperatures of an isotopic mixture containing 5% of hydrogenated 4-methyl-pyridine.

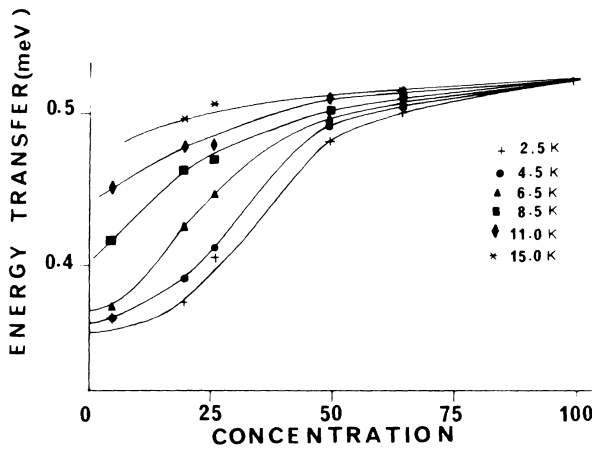


FIG. 4. Isothermal variation of the frequency at maximum intensity in isotopic mixtures of 4-methyl-pyridine and its perdeuterated derivative at different temperatures. The lines are guides for the eye. Concentrations are 4MP- h_7 %.

ic band decompositions may be misleading and the discussion will be concentrated on the frequencies at maximum intensities for the bands (Figs. 4 and 5).

(ii) At very low temperature (2.5 K) the band frequency is extremely sensitive to the isotopic dilution and decreases rapidly for 4MP- h_7 concentrations lower than 50% (Fig. 4). The frequency shift is rather smooth and indicates a progressive change of the methyl frequency. The bandwidth increases with the concentration of deuterated molecules and remains rather broad for the mixture containing 5% of 4MP- h_7 (Fig. 2).

(iii) The frequency shift at constant isotopic dilution is very sensitive to the temperature and almost disappears at 15 K (Figs. 4 and 5). This is in marked contrast with pure 4MP- h_7 , which shows no frequency shift with temperature (Fig. 5 and Ref. 17).

The different theories which have been proposed so far to describe the methyl-group dynamics in crystals at low

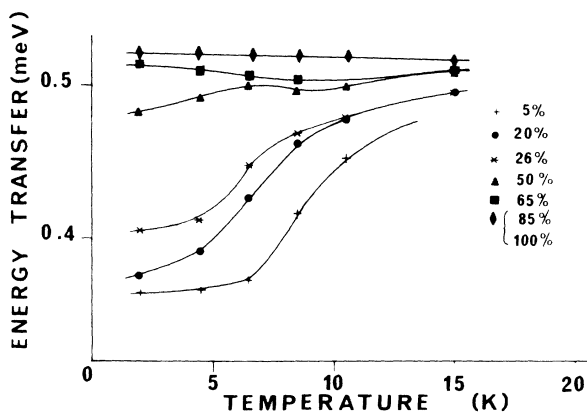


FIG. 5. Isoconcentration curves for the variation of the frequency at maximum intensity in isotopic mixtures of 4-methyl-pyridine and its perdeuterated derivative at different temperatures. The lines are guides for the eye. Concentrations are 4MP- h_7 %.

temperatures are (i) the isolated methyl group, (ii) pairs of coupled methyls, and (iii) coupling with lattice modes.

1. Isolated methyl groups

The simplest approach to methyl rotation is the isolated internal top experiencing a periodic potential. The corresponding Hamiltonian is

$$H_0 = -\frac{\hbar^2}{2I_r} \frac{\partial^2}{\partial \theta^2} + V(3\theta). \quad (1)$$

I_r is the reduced moment of inertia of the internal top, θ is the angular coordinate, and $V(3\theta)$ is a periodic potential consistent with the threefold symmetry of the methyl group. In this equation the kinetic coupling with the molecular frame is neglected. The potential may be expanded into a Fourier series:

$$V(3\theta) = \sum_i V_{3i}(3i\theta). \quad (2)$$

If one of the terms (usually V_3 or V_6) is dominant the eigen problem associated with the torsional motion may be transformed into the well-established Mathieu equation.^{18,19} Energy levels are labeled with two quantum numbers: the principal torsional quantum number for the harmonic oscillator limit ν and a sublevel index σ , which gives the symmetry or periodicity of the torsional wave functions. If the barrier is sufficiently low the degeneracy of the ν_σ sublevels is removed by tunneling. In the case of 4MP, the observed bands may then correspond to $0_0 \rightarrow 0_{\pm 1}$ transitions. The mean frequency of the low-resolution spectrum gives an estimate of the barrier height, either three or sixfold.^{5,8} This simple approach cannot account for isotope dilution and temperature effects in 4MP.

2. Pairs of coupled methyl groups

Pairs of strongly coupled methyl groups with their axes parallel to the c axis of the crystal are suggested by the crystal structure (Fig. 1). This model was proposed for lithium acetate ($\text{CH}_3\text{COOLi} \cdot 2\text{H}_2\text{O}$).²⁰⁻²² The corresponding Hamiltonian is

$$H_{12} = -\frac{\hbar^2}{2I_r} \left[\frac{\partial^2}{\partial \theta_1^2} + \frac{\partial^2}{\partial \theta_2^2} \right] + V_0(3\theta_1) + V_0(3\theta_2) + V_{12}(3(\theta_1 - \theta_2)), \quad (3)$$

where θ_1 and θ_2 are the angular coordinates for methyl groups. The two groups rotate in a static field V_0 around a common axis and are coupled together via an interaction potential V_{12} . This Hamiltonian is a particular case of a more general problem considering two coupled tops with nonparallel rotational axes.¹⁸⁻²³ There are 9 func-

tions belonging to the ground state ($w = v_1 + v_2 = 0$), 18 functions associated with the $w = v_1 + v_2 = 1$ state, etc. Each of these functions is a product of solutions of the single top problem that can be denoted $\langle v_{1\sigma_1}, v_{2\sigma_2} |$. For uncoupled methyls ($V_{12} = 0$), there are three distinct $w = 0$ energy levels, AA ($\langle 0_0, 0_0 |$), EA ($\langle 0_{\pm 1}, 0_0 |$ and $\langle 0_0, 0_{\pm 1} |$, fourfold), and EE ($\langle 0_{\pm 1}, 0_{\pm 1} |$, fourfold) at relative energies: 0, $h\nu_0$, and $2h\nu_0$; ν_0 being the tunneling frequency of the uncoupled methyl groups. The effect of the coupling term V_{12} is to shift the levels $\langle 0_0, 0_0 |$ and $\langle 0_{\pm 1}, 0_{\pm 1} |$ by -2δ and levels $\langle 0_{\pm 1}, 0_0 |$, $\langle 0_0, 0_{\pm 1} |$, and $\langle 0_{\pm 1}, 0_{\pm 1} |$ by δ .²⁰⁻²² This model was recently extended to include a possible methyl-methyl kinetic coupling that is represented by an additional term (proportional to $\partial^2/\partial\theta_1\partial\theta_2$) in the Hamiltonian [Eq. (3)].¹⁷ The AA and EA levels are unshifted, while the EE level is split. Therefore, a suitable combination of static and dynamical coupling may account for the different components observed in pure 4MP- h_7 .

In isotopic mixtures three different pairs must be considered:²² fully hydrogenated ($\text{CH}_3\text{-CH}_3$), fully deuterated ($\text{CD}_3\text{-CD}_3$), and mixed ($\text{CH}_3\text{-CD}_3$). In the absence of preferential pairing, between CH_3 and CD_3 , if p is the concentration of CH_3 groups, the concentration of the three different pairs are p^2 ($\text{CH}_3\text{-CH}_3$), $2p(1-p)$ ($\text{CH}_3\text{-CD}_3$), and $(1-p)^2$ ($\text{CD}_3\text{-CD}_3$). In the low-resolution limit, where the fine structure for each pair is not resolved, similar intensities for ($\text{CH}_3\text{-CH}_3$) and ($\text{CH}_3\text{-CD}_3$) pairs are expected for $p = 50\%$ (neutron scattering by CD_3 is neglected). In the corresponding mixture (Fig. 2) the rather broad band at $490 \mu\text{eV}$ might be due to two equal contributions of pure and mixed pairs. Therefore, the frequency shift for mixed pairs, with respect to fully hydrogenated pairs, should not exceed $30 \mu\text{eV}$. This is quite small compared to the frequency shift in the mixture containing 5% of 4MP- h_7 ($\sim 150 \mu\text{eV}$). An additional mechanism is necessary to account for this large frequency shift.

3. Coupling with lattice modes

The coupling of the methyl group rotor to lattice displacements (phonons) has been proposed to account for the shift of the tunneling frequency in isotopic mixtures of LiAc (Ref. 22) and for the temperature effect in methy-

liodide (CH_3I).²⁴ The corresponding Hamiltonian is written as

$$H = H_{12} + H_{\text{ph}} + H_{r\text{-ph}}, \quad (4)$$

where H_{12} corresponds to Eq. (3) and

$$H_{\text{ph}} = \sum_k \left[\frac{P_k^2}{2m_k} + \frac{m_k}{2} \omega_k^2 x_k^2 \right], \quad (5)$$

$$H_{r\text{-ph}} = \sum_k \left[\frac{2m_k \omega_k}{\hbar} x_k \right]^{1/2} \times \left[\frac{g_k^s}{\sqrt{2}} (\sin 3\theta_1 + \sin 3\theta_2) + \frac{g_k^c}{\sqrt{2}} (\cos 3\theta_1 + \cos 3\theta_2) \right]. \quad (6)$$

This Hamiltonian describes two rotors coupled to lattice modes (coordinate x_k , frequency ω_k). The coupling term proportional to g_k^s is called the "shaking" term. It decreases the effective potential barrier for the rotors. The coupling term proportional to g_k^c is called the "breathing" term. It increases the effective potential barrier.

At very low temperature, a thorough analysis of this Hamiltonian²² shows that the deuteration of one rotor in a pair increases the effective potential of the adjacent CH_3 group. Then a decreasing of the CH_3 tunneling frequency ratio ($\tau_{\text{CH}_3}/\tau_{\text{CD}_3}$) should be larger than the value calculated without change of the effective potential. The observed frequency for the hydrogenated and deuterated compounds is then a good indication of the change of the effective potential. For 4MP- h_7 and 4MP- d_7 the calculation of the potential functions in the single-particle approximation (Table I) shows that the barrier could be enhanced by 10–20% in 4MP- d_7 compared to 4MP- h_7 . However, the corresponding shift for the tunneling frequency of 4MP- h_7 diluted in 4MP- d_7 should be only 30–40 μeV , which is again very small compared to the 150 μeV observed for highly diluted samples.

Another consequence of rotor-phonon coupling is that the effective potential experienced by the methyl groups may depend on temperature, via the phonon state population. The "shaking" terms leads to a decreasing of the tunneling frequency with increasing temperature. This is

TABLE I. Single-particle potential barriers for 4-methyl-pyridine and its perdeuterated analogue at 5 K. V_3 and V_6 correspond to threefold and sixfold potentials, respectively.

	$\nu_{\text{calc}} (\text{cm}^{-1})$				
	$\nu_{\text{obs}} (\text{cm}^{-1})$	(a) $V_3 = 32 \text{ cm}^{-1}$	(b) $V_3 = 38 \text{ cm}^{-1}$	(a) $V_6 = 160 \text{ cm}^{-1}$	(b) $V_6 = 176 \text{ cm}^{-1}$
$\text{C}_6\text{H}_7\text{N}$	4.16	4.14	3.75	4.10	3.87
$\text{C}_6\text{D}_7\text{N}$	0.80	1.03	0.80	0.93	0.80

^aPotential scaled to the CH_3 frequency.

^bPotential scaled to the CD_3 frequency.

usually the most important. The “breathing” term, on the other hand, enhances the tunneling frequency at high temperature. In the case of pure 4MP- h_7 and 4MP- d_7 , there is no significant frequency shift with temperature and the coupling terms are certainly too small to account for the large temperature effects in isotopic mixtures.

This discussion points out that isotopic dilution and temperature effects are crucial aspects of the experiments presented in this work. They cannot be explained simply with the theoretical models previously proposed for methyl tunneling. At this stage, two different strategies can be considered. First, all the theoretical models reviewed so far are based on limited expansions of the Hamiltonian describing the methyl dynamics and it may be wondered whether higher-order terms are relevant. This would lead to rather complicated calculations. Alternatively, if it is suspected that the observed phenomena are so far from the known properties of the usual Hamiltonians that perturbative approaches are not relevant, then, a completely new theory, based on a new Hamiltonian, must be worked out. This is the purpose of Sec. II.

II. INFINITE CHAINS OF COUPLED METHYL GROUPS

Beside the close-contact pairs of methyl groups the crystal structure clearly indicates two sets of crystallographically equivalent infinite chains made of equidistant methyl groups, with their mean directions parallel to either a or b axes. The C—C bonds acting as rotor axes being perpendicular to the chain directions, the methyl groups are ideally positioned to behave like gear wheels and the CH₃-CH₃ distances of 4.0 Å are consistent with a coupling due to van der Waals interactions. Chains a and b do not cross each other since they are in different (a, b) planes. However, dynamical coupling of the chains may occur through the close-contact pairs parallel to the c crystal axis. Therefore, the methyl dynamics should be described by a local potential and coupling terms due to intrapair and intrachain interactions, respectively. Depending on the relative values for the coupling terms, different dynamical models should be considered: pairs of coupled methyl groups if the intrachain coupling is negligible, or isolated infinite chains of methyl groups if the intrapair coupling is negligible, or an infinite network of coupled rotors if both couplings are important.

A complete molecular-dynamics simulation would be necessary to estimate the coupling terms. This is beyond the scope of this paper. Nevertheless, it is possible to obtain qualitative information with simplified models for the crystal structure. Considering pairs of methyl groups along the c crystal axis (molecules labeled 1 and 2 on Fig. 1) or along the a or b directions (molecules labeled 4 and 4' or 1 and 3 on Fig. 1), proton-proton interactions can be represented by a pair potential of the Kitaigorodskii type:²⁵

$$E = -0.214 \left(\frac{2r_H}{d} \right)^6 + 47\,000 \exp \left[-12.34 \frac{d}{2r_H} \right], \quad (7)$$

E is in kcal/mol, r_H and d are in Å, respectively. Electrostatic and polarization effects are neglected. The methyl groups are assumed to be tetrahedral with C—H bond length of 1.1 Å and $r_H = 1.2$ Å.²⁵ Interaction energies were calculated by varying θ_2 while θ_1 was kept constant. In both cases, the coupling potentials are threefold and close to a $\cos 3\theta_2$ function. The barrier heights for nearest neighbors are 4.1 and 6.6 cm⁻¹ for the intrapair and intrachain potentials, respectively. These barriers are divided by about 100 and 10, respectively, for next-nearest neighbors with CH₃-CH₃ distance of 6 Å. These values must be considered with very strong reserves indeed, since the pair potential [Eq. (7)] does not include all the interactions in the crystal. However, these simple calculations suggest that neither of the two couplings can be neglected without further considerations. In Sec. I isolated pairs of coupled methyl groups have been considered. In this part, a theoretical approach for the dynamics of isolated chains of coupled methyl groups is proposed.

A. Theoretical model

The Hamiltonian describing a one-dimensional chain of coupled methyl groups (labeled j) is

$$H = \sum_j -\frac{\hbar^2}{2I_r} \frac{\partial^2}{\partial \theta_j^2} + \frac{V_0}{2} (1 - \cos 3i\theta_j) + \frac{V_c}{2} [1 - \cos 3i(\theta_{j+1} - \theta_j)]. \quad (8)$$

The first term represents the kinetic energy, the second term represents an “on-site” or external $3i$ -fold potential ($i = 1, 2, \dots$) that does not depend explicitly on lattice position and the last term is due to coupling (“strain” energy) between neighboring lattice sites. If $\theta_{j+1} - \theta_j$ is restricted to small amplitudes, then the coupling term can be linearized:

$$H \sim \sum_j -\frac{\hbar^2}{2I_r} \frac{\partial^2}{\partial \theta_j^2} + \frac{V_0}{2} (1 - \cos 3i\theta_j) + \frac{V_c}{2} \frac{(3i)^2}{2} (\theta_{j+1} - \theta_j)^2. \quad (9)$$

This Hamiltonian is equivalent to that of the sine-Gordon potential.²⁶⁻²⁷

As usual in quantum field theory,²⁷ it is worth beginning with the first approximation in which quantum effects are ignored and to treat this equation as if it were describing classical field configurations rather than quantum operators. Quantum mechanics may be regained by quantizing the classical solution through semiclassical [Wentzel-Kramers-Brillouin (WKB)] methods.²⁸

B. The classical sine-Gordon theory

In this section we follow the notation of Currie and co-workers.³² The classical sine-Gordon equation:

$$H_{SG} = LA \sum_j \frac{1}{2} \dot{\phi}^2 + \omega_0^2 (1 - \cos \phi_j) + \frac{1}{2} \frac{C_0^2}{L^2} (\phi_{j+1} - \phi_j)^2, \quad (10)$$

where L is the lattice constant, is equivalent to the classical version of Eq. (9) provided

$$\phi_j = 3i\theta_j, \quad (11)$$

$$A = \frac{I_r}{(3i)^2 L}, \quad (12)$$

$$\omega_0^2 = \frac{V_0(3i)^2}{2I_r}, \quad (13)$$

$$C_0^2 = \frac{V_c L^2 (3i)^2}{2I_r} = \omega_c^2 L^2. \quad (14)$$

In this system solitons, phonons, and breathers are the elementary excitations.

C. Continuous chains

If the coupling between sites is strong enough to ensure that variations of ϕ from site to site are quite small then the site index j can be replaced by a continuous position variable x so that ϕ becomes a continuous function of x and t (time): $\phi_j \rightarrow \phi(x, t)$. In this case, nonlinear kinks become well-defined elementary excitations with long lifetimes and as such behave very much like particles (solitons). The analytical form

$$\phi_{K\pm}(x, t) = 4 \arctan \left[\exp \left[\pm \frac{x - vt}{d(1 - v^2/C_0^2)^{1/2}} \right] \right], \quad (15)$$

$$d = \frac{C_0}{\omega_0} \quad (16)$$

describes kink (+) and antikink (-) solutions traveling

at velocity v . The "relativistic" Lorentz factor dependence on v appears also in the energy ($E_{K\pm}$) associated with a single kink:

$$E_{K\pm} = \frac{E_0}{(1 - v^2/C_0^2)^{1/2}}, \quad (17)$$

E_0 is the rest energy of the kink:

$$E_0 = 8A\omega_0 C_0 = 4(V_0 V_c)^{1/2}, \quad (18)$$

and the kink rest mass is given by

$$M_0 = \frac{E_0}{C_0^2} = \frac{8I_r}{(3i)^2 L^2} (V_0/V_c)^{1/2}. \quad (19)$$

In the present case, the kink carries the mean position of the methyl group from one minimum (say 0) of the local potential to another minimum (say $+2\pi/3i$) or vice versa for an antikink. The kinkwidth at rest is roughly $2d$. The rest energy is larger than the local potential barrier and the kink density vanishes at low temperature. Thus the kink signal in the INS spectra becomes negligible.

In addition to the large-amplitude spatially localized kinks, phonons (referred to as "rotons" in the present case) corresponding to small-amplitude oscillations are also solutions of the approximate Hamiltonian linearized with respect to a potential minimum:

$$H_L \sim LA \sum_j \frac{1}{2} \dot{\phi}_j^2 + \frac{1}{2} \omega_0^2 \phi_j^2 + \frac{1}{2} \frac{C_0^2}{L^2} (\phi_{j+1} - \phi_j)^2. \quad (20)$$

The continuum dispersion is

$$\omega_k^2 = \omega_0^2 + C_0^2 k^2. \quad (21)$$

The third kind of elementary excitation is composed of breathers or doublets which have the form

$$\phi_B(x, t) = 4 \arctan \left[\frac{(\omega_0^2/\omega_B^2 - 1)^{1/2} \sin[\omega_B(t - vx/C_0^2)/(1 - v^2/C_0^2)^{1/2}]}{\cosh[(x - vt)(1 - \omega_B^2/\omega_0^2)^{1/2}/d(1 - v^2/C_0^2)^{1/2}]} \right]. \quad (22)$$

The breather is traveling at velocity v ($v < C_0$) and its energy is given by

$$E_B = 2E_0 \frac{(1 - \omega_B^2/\omega_0^2)^{1/2}}{(1 - v^2/C_0^2)^{1/2}}. \quad (23)$$

E_0 is the kink rest energy [Eq. (18)] and ω_B is the frequency with which the breather envelope oscillates harmonically. In the classical limit this frequency varies continuously from 0 to ω_0 and as $\omega_B \rightarrow 0$ the breather amplitude approaches $2\pi/3i$ and its width approaches twice the soliton width. It decomposes to become a soliton-antisoliton pair. On the other hand, as $\omega_B \rightarrow \omega_0$ the breather profile becomes very extended and of low amplitude. Breathers can be viewed either as soliton-

antisoliton bound states or as anharmonic phonons. Arbitrarily low creation energies are possible for breathers and these excitations may contribute to the observed spectra at low temperature.

D. Discreteness effects

In a real discrete lattice the roton dispersion, the shape, and the dynamics of solitons and breathers are changed in several aspects.

The roton dispersion is

$$\omega_k^2 = \omega_0^2 + 4 \frac{C_0^2}{L^2} (\sin^2 \frac{1}{2} kL). \quad (24)$$

The continuum equation has the remarkable conservation property that soliton and breather excitations have infinite lifetimes. On the contrary, in the discrete problem, a traveling one-particle initial condition leads to a solution comprising both a particle and rotons (commonly referred to in this context as "radiation"). In the classical theory, the velocity of the particle decreases with time while the low-amplitude harmonic oscillations increase in number. The rotons are generated and provide viscous damping that draws energy and momentum from the traveling particle. The particle center is trapped in a particular unit cell.³⁷ The lowest potential configuration corresponds to lattice particles being symmetrically placed about the center of mass with no lattice particle at the center, while the highest potential configuration is again symmetric but with one lattice particle at the center. In the classical theory, this discrete lattice "pinning effect" is found to modulate sinusoidally the velocity of propagation and the pseudoparticle position with a frequency ω_0 and an amplitude nearly proportional to ω_0 over the range of ω_0 for which propagation is possible. The pinning potential depends on the particle width. If the width is large compared to the lattice parameter then the difference between the two extreme configurations is weak. In any case, owing to the Lorentzian contraction of the pseudoparticle, the width may become small for large velocities and pinning results.

E. The quantum sine-Gordon theory

Dashen and co-workers²⁸ have applied to quantum field theory the semiclassical or WKB method. The chain is supposed to be a large closed loop with a perimeter of length NL and periodic boundary conditions. In order to eliminate some divergences in summations it is necessary to renormalize the mass of the particles. This accounts for the kink interactions with phonons that modify the zero-point energy. The kink (antikink) of the classical sine-Gordon potential turns into quantum-mechanical particles with a rest mass:

$$M_k = M_0 \left(1 - \frac{g^2}{8\pi} \right), \quad (25)$$

$$g = 3i. \quad (26)$$

The renormalized mass M_k is interpreted as the observable rest mass, as opposed to the bare mass M_0 of the classical kink [Eq. (19)].³⁰

The quantization of the classical breather solution [Eq. (22)] yields a discrete spectrum of particle masses:

$$M_B(l) = 2M_0 \left(1 - \frac{g^2}{8\pi} \right) \sin \frac{lg^2}{16(1-g^2/8\pi)} \\ l = 1, 2, \dots < \frac{8\pi}{g^2} - 1. \quad (27)$$

The crucial role played by g in this equation is a consequence of the quantization of the sine-Gordon Hamiltonian.³⁵ In classical physics changing g amounts to multiplying the Hamiltonian by a constant. This has no effect on the physics other than redefining the energy scale. On

the other hand, in the quantum theory the energy scale is determined by \hbar/g^2 and energy rescaling due to a change of g is equivalent to rescaling Planck's constant h . This is somewhat obscured in theoretical works since units are usually chosen such that $\hbar=1$. The zero-point vacuum energy of the quantum system (mass renormalization) and the number of stationary states above this lower limit are related to g . For very low g (weak-coupling limit) the renormalization factor is nearly unity and the system is close to the classical limit. There is a large number of mass states for the breather. As g increases the mass states disappear one by one and decay into soliton-antisoliton pairs; when the l th state disappears ($l=8\pi/g^2-1$) $E_B(l)$ is twice the soliton energy. The $l=1$ state is the fundamental breather state and $2E_K - E_B(1)$ is the activation energy for the creation of a soliton-antisoliton pair at rest. For $g^2 \geq 8\pi$ the lowest state breaks up and disappears from the spectrum. The renormalization factor become negative and the theory is physically meaningless. This is of importance in the case of methyl groups: the quantum sine-Gordon theory is relevant only for the threefold potential. Then, there is only one mass state for the breather ($l=1$) and this is the fundamental state.

According to Eqs. (23) and (27) the classical harmonic frequency of the breather is

$$\omega_B(l) = \omega_0 \cos \frac{lg^2}{16(1-g^2/8\pi)}. \quad (28)$$

In the WKB theory the renormalized energy spectrum of the breather is

$$E_{n,l} = [E_B^2(l) + p_n^2 C_0^2]^{1/2} \quad n = 0, \pm 1, \pm 2, \dots, \pm \infty, \quad (29)$$

where p_n is the center-of-mass momentum of the breather. There is thus a finite set of particles (labeled l) with masses $M_B(l)$ that propagate for discrete momentum values p_n .

F. Tunnel effect

Another important aspect of quantization is the cancellation of the classical ground-state degeneracy yielding a tunnel effect and level splitting. The methyl tunneling problem in the infinite chain of coupled groups is now a one-dimensional band-structure problem.³² The eigenvalues are labeled $E_{v_\sigma, k}$ with a band index v_σ and a wave vector k . (In the first Brillouin zone $-g/2 < k \leq g/2$.) The corresponding eigenfunctions have the Bloch form

$$\psi_{v_\sigma, k}(\theta) = \exp(ik\theta) u_{v_\sigma, k}(\theta) \quad (30)$$

with

$$u_{v_\sigma, k} \left[\theta + \frac{2\pi}{g} \right] = u_{v_\sigma, k}(\theta). \quad (31)$$

By putting these eigenfunctions into Eq. (8) it appears that tunnel splitting may occur only when the eigenfunction has Fourier components of the same periodicity as the potential terms. This is the case at the zone center ($k=0$), where the methyl groups are in phase and at the

zone boundary ($k = g/2$), where the methyl groups are out of phase. The eigenproblem then reduces to an analysis of the corresponding Mathieu equations:

$$\left[-\frac{\hbar^2}{2I_r} \frac{\partial^2}{\partial \theta^2} + \frac{V_0}{2}(1 - \cos g\theta) \right] \psi(\theta) = E \psi(\theta), \quad (32)$$

$$\left[-\frac{\hbar^2}{2I_r} \frac{\partial^2}{\partial \theta^2} + \frac{V_0}{2}(1 - \cos g\theta) + \frac{V_c}{2}(1 - \cos 2g\theta) \right] \psi(\theta) = E \psi(\theta). \quad (33)$$

G. Methyl dynamics and inelastic neutron scattering

In the single-particle approach, the periodic potential manifests itself through tunneling and rotational transitions. The former corresponds to permutations of the hydrogen atoms, whereas the latter are related to small-amplitude oscillations around the equilibrium position, when the potential barrier is high. In the infinite chain, the dynamics is rather different and much richer. The rotational motion of the single particle turns into a continuum of roton states [Eq. (24)]. This is the usual correspondence between isolated vibrations and coherent excitations in crystals. Similarly, the tunneling of the single particle gives coherent tunneling for the whole chain. However, there is no continuum of states: only in-phase and out-of-phase permutations of the protons are allowed by the symmetry translation of the chain [Eqs. (32) and (33), respectively].

In addition to these coherent excitations, spatially localized incoherent excitations may occur in the chain. Traveling solitons (antisolitons) achieve progressive permutations of the protons along the chain [Eq. (15)]. This may be compared to classical jumping above the potential barrier for the single particle. In both cases, these processes are thermally activated and occur only at high temperature. The breather, on the other hand, has no parent for single particles. As a soliton-antisoliton bound pair it can be seen as the preliminary step for the creation of a soliton and antisoliton pair. Alternatively, as a superposition of roton states, it corresponds to spatially localized oscillations of the methyl groups around their equilibrium positions.

Coherent and incoherent excitations can be distinguished by INS. For 4MP- h_7 , the relative proportions of scattered neutrons are $\sim 9\%$ (coherent) and 91% (incoherent). For the deuterated derivative, these values turn into 84% (coherent) and 16% (incoherent). Therefore, the incoherent modes in 4MP- h_7 are ten times more intense than the coherent modes, whereas for MP- d_7 the incoherent modes are five times weaker than the coherent modes.

III. TUNNELING AND BREATHERS IN PURE 4MP

The spectra of pure 4MP- h_7 and 4MP- d_7 can be interpreted in terms of tunneling and breather modes in a threefold quantum sine-Gordon potential. The weaker bands at 535 and $468 \mu\text{eV}$ in 4MP- h_7 are assigned to in-

phase and out-of-phase tunneling transitions, respectively. The corresponding sine-Gordon potential is then completely determined according to Eqs. (32) and (33) (Table II). Two tunneling transitions at 141 and $74 \mu\text{eV}$ are expected in the d_7 compound. These two bands are not resolved (Fig. 3 and Ref. 8). However, the observed transition at $100 \mu\text{eV}$ corresponds well to the mean value. The soliton and the breather envelope at rest are represented in Fig. 6 and their characteristic values are gathered in Table III. The renormalized rest energy of the breather [17.64 meV (142.16 cm^{-1})] and the minimum energy required for the creation of a soliton-antisoliton pair at rest [22.95 meV (185 cm^{-1})] yield an activation energy [$\sim 5.33 \text{ meV}$ (43 cm^{-1})] that makes the soliton population practically zero in the present experiments below 15 K . The internal frequency of the breather is the only value depending on the isotopic substitution.

Once the rest energy of the breather is determined then the energy spectrum can be calculated. The breather may be seen as a free particle in a periodic medium. Because of the translational symmetry, steady propagation occurs only if the associated de Broglie wavelength is an integer fraction of the lattice parameter:

$$\lambda = \frac{1}{p_n} = \frac{L}{n} \quad n = 0, \pm 1, \pm 2, \dots, \quad (34)$$

and

$$E_{l,n} = [E_B(l)^2 + n^2 \omega_c^2]^{1/2}. \quad (35)$$

The calculated and observed breather spectra are in good agreement (Tables IV and V for h_7 and d_7 molecules, respectively). The weak band near $220 \mu\text{eV}$ in the 5% 4MP- h_7 mixture (Fig. 3) may correspond to the $n = 0 \rightarrow 1$ transition calculated for 4MP- d_7 [1.8 cm^{-1} ($223 \mu\text{eV}$) in Table V]. As expected, the relative intensities for the breather (incoherent) and tunneling (coherent) excitations are quite different in 4MP- h_7 and 4MP- d_7 .

Small differences between observed and calculated frequencies may be due to the perturbation of the wave forms in the real lattice. In the discrete lattice, particles are narrower than the continuum particles propagating at the same velocity^{36,37} and the real waveform of the soliton and breather may differ slightly from those shown in

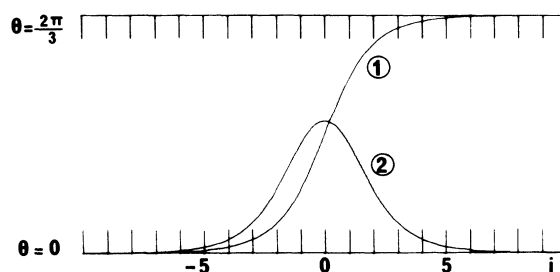


FIG. 6. Waveforms for the soliton (1) and for the envelope of the semiclassical breather in the lowest mass state (2) at rest in the sine-Gordon potential: $V(\theta_j) = \frac{29.5}{2}(1 - \cos 3\theta_j) + \frac{44}{2}[1 - \cos 3(\theta_{j+1} - \theta_j)]$; V and θ_j are in cm^{-1} and radian units, respectively.

TABLE II. Observed and calculated frequencies for the methyl rotation in the sine-Gordon potential: $V(\theta_j) = \frac{29.5}{2}(1 - \cos 3\theta_j) + \frac{44}{2}[1 - \cos 3(\theta_{j+1} - \theta_j)]$; V and θ are in cm^{-1} and radian units. An asterisk denotes doubly degenerate levels.

4MP- h_7				4MP- d_7			
in-phase		out-of-phase		in-phase		out-of-phase	
obs.	calc.	obs.	calc.	obs.	calc.	obs.	calc.
4.31	4.31*	3.77	3.77*	0.8	1.14*	0.8	0.60*
	26.74*		27.94*		17.75*		22.26*
	52.12		45.64		27.16		27.10
	54.21		66.69		31.13		42.11
	92.04*		95.22*		47.30*		58.83*

Fig. 6. The calculated potential energy in the discrete lattice for the continuum breather [16.54 meV (133.3 cm^{-1})] is lowered by about 10%. The perturbation of the wave form is probably of the same order. The calculated energy spectrum (Tables IV and V) with this value is also in good agreement with the observation: the experimental values are between the calculated ones with the continuous and discrete rest energies. According to Eq. (35), the observed spectrum may provide an estimate of the “real” energy at rest for the breather [16.52 meV (133.1 cm^{-1}), Tables IV and V]. This “exact” value will be used in Sec. IV, where calculated and experimental spectra are compared.

A numerical calculation shows that the pinning potential is about $5 \times 10^{-4} \text{ cm}^{-1}$ for the breather and pinning is not likely to play an important role. In the excited states the breather velocity remains small compared to C_0 and relativistic effects are negligible (Tables IV and V).

At very low temperature, the spectrum is dominated by fundamental transitions ($0 \rightarrow 1$, $0 \rightarrow 2$, etc., Table IV).

At higher temperature, excited states are populated and hot transitions [specifically the $1 \rightarrow 2 \sim 1.39 \text{ meV}$ (11 cm^{-1})] appear. Between 0 and 15 K, the population of $n \geq 2$ states is negligible and the intensity of the $0 \rightarrow 1$ transition is expected to decrease as $[1 - \exp(h\nu_{01}/kT)]$. It is roughly divided by 2 between 2.5 and 10 K. This is in qualitative agreement with the experiments.¹⁷

IV. BREATHER DYNAMICS IN ISOTOPIC MIXTURES

In isotopic mixtures of 4MP- h_7 and 4MP- d_7 , the molecules are completely miscible and distributed randomly among the crystal sites. In the temperature range of the experiments, i.e., far below the melting point, there is no molecular migration nor chemical exchange between hydrogen atoms and deuterium atoms. Therefore, h_7 and d_7 molecules are distributed into clusters of various sizes (s_h and s_d , respectively) determined by simple combinatorial statistics and unaffected by temperature. The observed bandwidth and frequency are related to the breather dynamics in the cluster distribution at a given

TABLE III. Soliton and breather modes in the sine-Gordon potential: $V(\theta_j) = \frac{29.5}{2}(1 - \cos 3\theta_j) + \frac{44}{2}[1 - \cos 3(\theta_{j+1} - \theta_j)]$; V and θ are in cm^{-1} and radian units, respectively. L is the lattice parameter.

4MP- h_7	4MP- d_7	
5.6	2.66	Rotational constant $F = h^2/8\pi^2 I_r$ (cm^{-1})
27.27	18.79	$\hbar\omega_0$ (cm^{-1})
33.30	22.95	$\hbar\omega_c$ (cm^{-1})
1.22	1.22	d/L : particle width parameter.
144.11	144.11	E_0 (cm^{-1}): rest energy of the classical soliton.
92.51	92.51	E_k (cm^{-1}): renormalized rest energy of the semiclassical soliton.
6.89	13.78	M_K (amu): renormalized rest mass of the semiclassical soliton.
142.16	142.16	$E_B(1)$ (cm^{-1}): renormalized rest energy of the semiclassical breather.
10.59	21.18	$M_B(1)$ (amu): renormalized rest mass of the semiclassical breather.
17.45	12.03	$\hbar\omega_B$ (cm^{-1}): frequency of the envelope of the semiclassical breather at rest in the fundamental state.
1.17	1.17	Maximum amplitude (in radian units) of the semiclassical breather envelope.

TABLE IV. 4-methyl-pyridine. Observed and calculated frequencies for the traveling breather in the sine-Gordon potential: $V(\theta_j) = \frac{29.5}{2}(1 - \cos 3\theta_j) + \frac{44}{2}[1 - \cos 3(\theta_{j+1} - \theta_j)]$; V and θ are in cm^{-1} and radian units, respectively. n is the kinetic quantum number, v the particle velocity, and d/L is the particle width parameter in lattice parameter units. N denotes neutron scattering; R denotes Raman scattering after Ref. 10.

n	Breather				v/C_0	$(1-v^2/C_0^2)^{1/2}$	d/L
	obs.	a	b	c			
0		0.0	0.0	0.0	0.0	1.0	1.22
1	4.1 N	3.8	4.5	4.1	0.24	0.97	1.18
2	15.3 N	14.6	17.1	15.7	0.45	0.89	1.09
3	31.7 R	31.1	35.8	33.3	0.60	0.80	0.98
4	55 R	51.9	58.9	55.2	0.71	0.71	0.87
5		79.5	84.7	80.0	0.78	0.62	0.76

^aContinuous approximation.

^bDiscrete approximation.

^cExperimental fit.

concentration and to the thermally populated states at a given temperature.

A. Breather in a box

Although isotopic mixtures of 4MP- h_7 and 4MP- d_7 molecules form a homogeneous crystal from the structural viewpoint, clusters of h_7 and d_7 molecules form a very inhomogeneous medium for the breather dynamics. The strain frequency ω_0 and the speed C_0 are divided by $\sqrt{2}$ in d_7 clusters with respect to h_7 clusters. Therefore, even if the energy at rest of the breather is not affected by deuteration (Table III) the internal frequency and the traveling speed are dramatically reduced. Numerical simulations^{36,37} show that solitons may adjust potential and kinetic energies when traveling through impurities. However, the situation may be different for breathers that are characterized by spatial and temporal coherence. Although no theoretical analysis of the breather dynamics in finite chains is available, it may be suspected that the relationship between the dynamics and the impurity distribution is not trivial. A simple approach is to suppose that deuterated clusters play the role of reflective walls

for breathers in h_7 clusters, and vice versa. Boxes of finite length (sL) have thus to be considered. Strictly speaking, breathers extend from $-\infty$ to $+\infty$ and it is not clear whether it is justified in searching for breathers in a medium of finite length. However, Dashen and co-workers²⁸ have conjectured that the sine-Gordon equation still acts like an exactly separable system in boxes of finite length. The renormalization remains unchanged. This is why the WKB method in a closed loop chain yields exact results. Therefore, we shall assume that quantum pseudoparticles in boxes may exist, and their rest energies are not significantly dependent on the size of the box. The main change due to the finite character of the chain is that the ground state no longer corresponds to the breather at rest. According to the uncertainty principle the minimum momentum value is $p_s = (1/sL)$. The relative energy of the ground state in a cluster with respect to the fundamental state in an infinite chain is then

$$E_{l,s} = [E_B^2(l) + \omega_c^2/s^2]^{1/2} \quad s = \pm 1, \pm 2, \dots \quad (36)$$

In the excited traveling states, Eq. (35) with $n \geq 1$

TABLE V. Deuterated 4-methyl-pyridine. Observed and calculated frequencies for the traveling breather in the sine-Gordon potential: $V(\theta_j) = \frac{29.5}{2}(1 - \cos 3\theta_j) + \frac{44}{2}[1 - \cos 3(\theta_{j+1} - \theta_j)]$; V and θ are in cm^{-1} and radian units, respectively. n is the kinetic quantum number; v the particle velocity, and d/L is the particle width parameter in lattice parameter units. N denotes neutron scattering; R denotes Raman scattering after Ref. 10.

n	Breather				v/C_0	$(1-v^2/C_0^2)^{1/2}$	d/L
	obs.	a	b	c			
0		0.0	0.0	0.0	0.0	1.0	1.22
1	1.8 N	1.8	2.2	2.0	0.17	0.99	1.20
2		7.1	8.4	7.7	0.33	0.95	1.15
3	21 R	15.6	18.2	16.8	0.46	0.89	1.08
4	32 R	26.8	30.8	28.6	0.57	0.82	1.00
5	44 R	40.1	45.9	42.7	0.65	0.76	0.92

^aContinuous approximation.

^bDiscrete approximation.

^cExperimental fit.

remains valid. This is because the box size is always an integer multiple of the lattice parameter. Therefore, the de Broglie wavelength of the particle is an integer fraction of the lattice parameter and of the box length as well.

The transition frequencies for a breather in a box are then

$$\nu_{sn} = [E_B^2(l) + n^2\omega_c^2]^{1/2} - [E_B^2(l) + \omega_c^2/s^2]^{1/2}. \quad (37)$$

Numerical values (Table VI) show that when the cluster size decreases then the energy of the ground state, with respect to that of the infinite chain, increases and the $0 \rightarrow 1$ transition frequency decreases. This is in qualitative agreement with the data (Figs. 2 and 4). Moreover, the band frequency observed in the most dilute sample [$360 \mu\text{eV}$ (2.90 cm^{-1}) in 5% 4MP- h_7] is in good agreement with that predicted for clusters including only two h_7 sites [$380 \mu\text{eV}$ (3.06 cm^{-1})]. The discrepancy is about 5% and this is of the order of the possible change of the effective potential due to deuteration (Table I). If this remarkable agreement is not due to a fortuitous cancellation of large errors, it confirms that the rest energy of the breather is only very slightly affected by the box size. For the minimum cluster size ($s=1$) the lowest state corresponds to the first excited state ($n=1$) in the infinite chain. The existence of breathers in such minimal clusters is questionable. Fortunately, in this case, the lowest transition is expected at 11 cm^{-1} , i.e., far from the frequency range considered in the present experiments and one-site clusters do not contribute to the observed spectra. Large clusters, on the other hand, are quite similar to infinite chains. Practically, for $s > 10$, the frequency shift is within the experimental errors. This corresponds roughly to twice the breather width.

To describe completely the energy levels of adjacent h_7 and d_7 clusters it is necessary to account for their different zero-point energies. The renormalization factor being the same for h_7 and d_7 breathers, the difference is $(\frac{1}{2})\hbar(\omega_{0h} - \omega_{0d})$ (i.e., $525 \mu\text{eV}$ (4.23 cm^{-1})), Table III. There is no state coincidence on the energy-level diagram (Fig. 7) and breathers may go through the different clusters only by tunneling. This tunneling is likely to depend

TABLE VI. Calculated relative energies (in cm^{-1} unit) in the fundamental states ($E_{0s} - E_0$) and transition frequencies ($E_1 - E_{0s}$) for the breather in boxes of length sL .

s	4MP- h_7		4MP- d_7	
	$E_{0s} - E_0$	$E_1 - E_{0s}$	$E_{0s} - E_0$	$E_1 - E_{0s}$
1	4.10	0.00	1.97	0.00
2	1.04	3.06	0.49	1.48
3	0.46	3.64	0.22	1.75
4	0.26	3.84	0.12	1.85
5	0.17	3.93	0.08	1.89
6	0.12	3.98	0.05	1.92
7	0.09	4.01	0.04	1.93
8	0.07	4.03	0.03	1.94
9	0.05	4.05	0.02	1.95
10	0.04	4.06	0.02	1.95

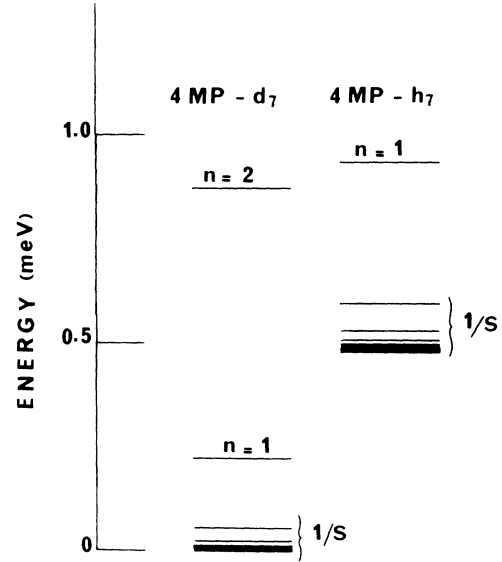


FIG. 7. Relative energy levels of the breathers in h_7 and d_7 clusters of 4-methyl-pyridine. n is the kinetic quantum number. S is the cluster size in lattice units.

on the minimum kinetic energy in the ground state (i.e., on the h_7 or d_7 cluster size) and on the barrier width (i.e., on the size of the adjacent d_7 or h_7 cluster).

B. Cluster size statistics

A complete analysis of the cluster size distribution in an infinite chain of randomly substituted lattice sites is not necessary since the incoherent scattering process in a cluster is independent of the cluster distribution along the rest of the chain. (Possible tunneling is neglected for the moment.) Considering neutrons scattered by protons, the intensity is proportional to the concentration p of h_7 molecules ($1-p$ for d_7). The probability for a given lattice site to belong to a cluster made of s contiguous h_7 molecules with one d_7 molecule at each end is

$$P(s) = p^s(1-p)^2. \quad (38)$$

Here it is supposed that one d_7 molecule on each side is enough to isolate completely the h_7 cluster. The transition frequency of the breather is ν_s and the scattered intensity is

$$I_s = sp^s(1-p)^2. \quad (39)$$

After removing the one-site clusters that are out of the frequency range, the total intensity is

$$\sum_{s>1} I_s = p - p(1-p)^2. \quad (40)$$

Owing to the spectral resolution and to the intrinsic bandwidth, clusters larger than a certain threshold size S cannot be distinguished. They all merge into a single band, the intensity of which is

$$I_S = p - \sum_{s=1}^S sp^s(1-p)^2. \quad (41)$$

The mean frequency depends on the isotopic concentration as

$$\bar{\nu}_p = \sum_{s>1} \nu_s I_s . \quad (42)$$

Calculated spectra (Fig. 8) are in good agreement with the experiment (Fig. 2) and the observed frequency shift can be assigned mainly to the variation of the cluster size distribution with the isotopic concentration. However, there are some differences between calculation and observation. The relative intensity of the low-frequency band [near 370 μeV (3 cm^{-1})] is overestimated and the calculated mean frequency does not agree with the experiment. Moreover, the low-frequency band appears better resolved on calculated spectra than on the experimental ones. These differences are believed to come from the crude approximation in the cluster distribution and do not preclude the validity of the interpretation based on the quantum sine-Gordon theory.

The previous calculation may be improved if fast exchange between clusters, probably due to tunneling, is considered. It is supposed that for a given h_7 cluster of size s_h , only d_7 clusters of size $s_d \geq r(s_h)$ behave like reflective walls, whereas for $s_d \leq r(s_h)$ d_7 clusters are

transparent for h_7 breathers. Then, Eq. (38) is rewritten as

$$P(s) = p^s (1-p)^{2r(s)} . \quad (43)$$

Because of the lack of quantitative information on the breather tunneling, $r(s_h)$ may be represented by the same step function for all s_h :

$$r(s_h) = \begin{cases} r_0, & s_h \leq S_0 \\ l, & s_h > S_0 . \end{cases} \quad (44)$$

The best fit (Fig. 9, $T=2.5 \text{ K}$) was obtained with $r_0=4$ and $S_0=4$. This means that a d_7 cluster becomes a purely reflective wall when its size is of the order of the breather width. These are only average values and the real exchange mechanism is certainly much more complicated. A theoretical model would be necessary to pursue more sophisticated analyses of the data.

C. Temperature effect

In the breather energy diagram (Fig. 7) there is no state coincidence for adjacent h_7 and d_7 clusters at very low temperature. When the temperature increases, roton states are thermally populated and a continuum of breather-roton states appears according to Eq. (24). If the temperature is sufficiently high, breather-roton states in adjacent clusters may coincide and lower their total kinetic energy to merge into a single breather at rest, or nearly so, extending over the two clusters. Both spatial and temporal coherence of the new breather can be achieved through interactions with rotons, which should also remove the excess kinetic energy. This is possible only if the thermal energy is sufficiently larger than the difference of zero-point energies for h_7 and d_7 domains [i.e., $\sim 500 \mu\text{eV}$ (4 cm^{-1}), Fig. 7]. Then, these energy differences become small fluctuations that can be counterbalanced by rotons.

This thermally activated process can be modeled with a first-order law assuming that there is an activation energy E_a , with respect to the zero-point energy of d_7 clusters. A d_7 breather-roton state at $E \geq E_a$ is incorporated into an h_7 breather-roton state to form a breather at rest and rotons, whereas for $E < E_a$ there is no breather interaction across clusters, except through tunneling [Eq. (44)]. Therefore, populating breather-roton states at $E \geq E_a$ is formally equivalent to decreasing the concentration of d_7 sites in the chain:

$$P(T) = p + (1-p)(1 - e^{-E_a/kT}) . \quad (45)$$

This approach is consistent with the experiments (Figs. 9 and 10) and the estimated activation energy ($E_a \sim 9 \text{ cm}^{-1}$) is about twice the zero-point energy difference for h_7 and d_7 clusters. The real physics is certainly more complicated since the activation energy probably depends on the exact size of the adjacent clusters and it is not possible to say whether this relationship is purely phenomenological.

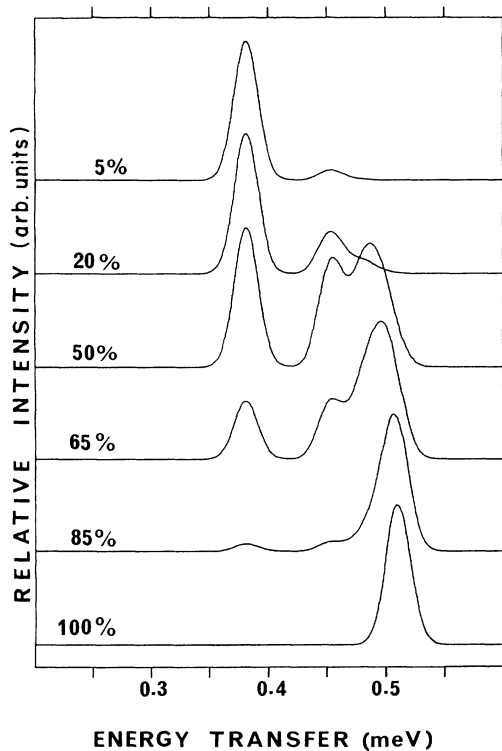


FIG. 8. Calculated spectra for the breather in isotopic mixtures of 4-methyl-pyridine and its perdeuterated derivative at 2.5 K. Each transition is convoluted with a Gaussian profile with a full width at half height of 15 μeV . The concentration (%) in h_7 derivative is shown on each curve.

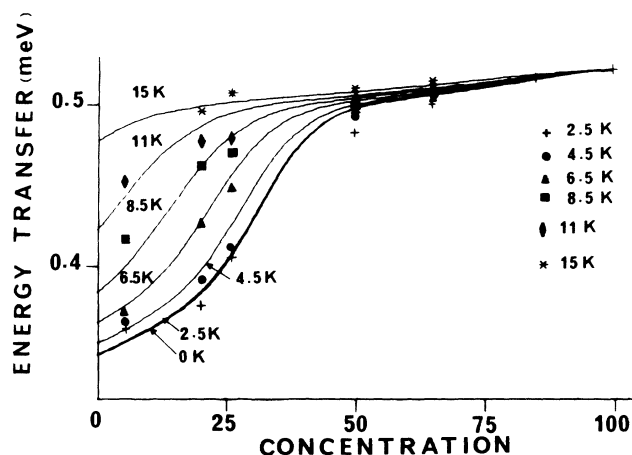


FIG. 9. Calculated isothermal curves for the mean frequency of the breather (—) and experimental frequencies at maximum intensity in isotopic mixtures of h_7 and d_7 4-methylpyridine. The calculated frequencies are rescaled ($X \sim 1.1$) to the experimental data. Concentrations are 4MP- h_7 %.

V. GENERAL DISCUSSION

The rather good agreement of the calculated curves with experimental data (Figs. 9 and 10) shows that the methyl dynamics in 4MP is well described by the sine-Gordon Hamiltonian for an isolated chain and there is no real need to introduce further interchain coupling in order to improve the fitting. The coupling term ($V_c = 22 \text{ cm}^{-1}$, Table II) appears much larger than the value calculated ($\sim 6 \text{ cm}^{-1}$) with Eq. (7), which turns out to be a poor approximation. Electrostatic and polarization terms should be included in a more realistic calculation. The value estimated for the coupling in close-contact pairs ($\sim 4 \text{ cm}^{-1}$) is then probably underestimated. It

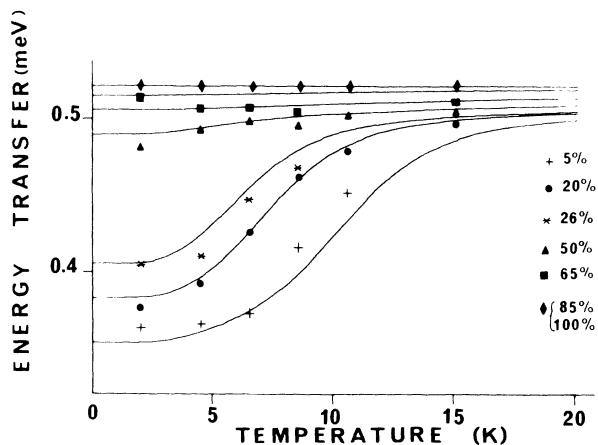


FIG. 10. Calculated isoconcentration curves for the mean frequency of the breather (—) and experimental frequencies at maximum intensity in isotopic mixtures of h_7 and d_7 4-methylpyridine. The calculated frequencies are rescaled ($X \sim 1.1$) to the experimental data. Concentrations are 4MP- h_7 %.

seems reasonable to suppose that intrachain and interchain couplings could be of the same order of magnitude but with different consequences on the methyl dynamics. According to field theory,²⁷ in systems with dimension greater than one, additional degrees of freedom have to be used in order to support solitons and breathers. In the case of methyl rotation, if there is no physical basis for such additional degrees of freedom, solitons or breathers should be confined in one-dimensional chains, even though interchain and intrachain couplings are of the same order.

A physical picture to understand why interchain coupling may have no effect on the one-dimensional breather dynamics may be sought in the ideal sine-Gordon case for which breathers and rotons are completely separable excitations. The internal frequency for the breather at rest (ω_B) is within the roton energy band [Eq. (24)]. Chains a and b being crystallographically equivalent, any breather in chain a can be associated with a phonon in chain b , or vice versa, such that the two methyl groups in the close-contact pair that these two chains have in common oscillate at the same frequency. This is required to ensure the stability of the breather. In the first excited traveling state, relativistic corrections are small and the breather can propagate steadily. In higher excited states, the internal frequency may become quite large and fall out of the roton energy bands. Then, the close-contact pairs would give rise to damping that slows down the breather. This would give band broadening in the spectra.

Even if it is relevant to think that interchain coupling has no effect on the breather dynamics in pure 4MP, this coupling is probably responsible for some of the observations in isotopic mixtures. As a matter of fact, whereas the energy levels (Fig. 7) suggest that a single CD_3 group should be a reflexive impurity for the breather in a CH_3 cluster, the rather small frequency shift observed for the 50% mixture (Fig. 2), where there are 50% of $\text{CH}_3\text{-CD}_3$ pairs, suggests that mixed pairs are almost transparent for the breather propagation along the chains. It is likely that a CD_3 group in a given chain has different dynamics depending upon whether it is in a $\text{CD}_3\text{-CH}_3$ or in a $\text{CD}_3\text{-CD}_3$ pair along the c axis. Intrachain coupling may thus be hidden in our assumptions concerning the cluster size threshold for breathers in 4MP- h_7 clusters to go through 4MP- d_7 clusters. For the same reasons, interchain coupling may also contribute to the bandwidth in isotopic mixtures (Fig. 2).

Previous Raman data¹⁰ were interpreted in terms of collective oscillations of the methyl groups. Raman bands at low frequency due to methyl groups were clearly identified by their frequency shifts upon deuteration, which are quite different from those expected for the lattice modes. Now, these transitions can be reconsidered on the basis of the sine-Gordon theory. The observed frequencies up to 6.82 meV (55 cm^{-1}) (Table IV) correspond rather well to transitions to upper traveling states for the breather. Besides, a phase transition was indicated near 100 K .¹⁰ Above this temperature methyl groups are freely rotating. The phase transition is monitored by a lattice mode at 7.6 meV (61 cm^{-1}). When excited states of this phonon are thermally populated, the potential terms (V_0

and V_c) are canceled. This is indicative of “shaking” type terms in the Hamiltonian [Eq. (6)]. The activation energies for crystal disordering and for creation of soliton-antisoliton pairs [~ 5 meV (40 cm $^{-1}$)] are thus similar in 4MP. The two phenomena occur simultaneously and the density of soliton-antisolitons is likely to remain small.

If traveling breathers are real in 4MP, is there any change to observe similar excitations in other crystals containing weakly hindered methyl groups? To a large extent, interpretations of methyl tunneling spectra are based on the measurements of frequency ratios for hydrogenated and deuterated materials. An important consequence of the sine-Gordon theory is that the most intense bands for hydrogenated and deuterated compounds may not correspond to the same kinds of excitations. Traveling breathers give the most intense incoherent signal in the former, while coherent tunneling transitions are enhanced by deuterium. Therefore, the apparent frequency ratio given by the most intense features may be misleading and it was indeed in a previous work on 4MP.⁸ The sine-Gordon theory provides good reasons to reconsider previous data and to complete some earlier experiments. Apart from 4MP, lithium acetate is the most thoroughly studied system and a large amount of experimental data seems to be consistently understood in terms of “isolated” close-contact pairs of coupled methyl groups.²⁰⁻²² However, the data can be rationalized with the sine-Gordon theory as well (Table VII). The spec-

trum of the fully hydrogenated sample show three peaks in the 200- μ eV region. The weaker bands at 214 μ eV (1.725 cm $^{-1}$) and 250 μ eV (2.015 cm $^{-1}$) can be assigned to the coherent tunneling (out of phase and in phase, respectively) and V_0 and V_c are determined accordingly. Then the $0 \rightarrow 1$ transition for the traveling breather is calculated at 283 μ eV (2.278 cm $^{-1}$), which corresponds to the most intense band. The frequency calculated for the deuterated breather [142 μ eV (1.142 cm $^{-1}$), Table 7] may correspond to the band at 130 μ eV (1.048 cm $^{-1}$) in diluted mixtures. In isotopic mixtures, the calculated breather frequency shifts down to 212 μ eV (1.706 cm $^{-1}$) for CH $_3$ clusters of minimum size. This may correspond to the broad band around 180 μ eV (1.451 cm $^{-1}$). The situation is less clear for the tunneling transitions in the fully deuterated sample that are calculated at 41 μ eV (0.330 cm $^{-1}$) and 21 μ eV (0.181 cm $^{-1}$) for the in-phase and out-of-phase modes, respectively, whereas transitions are observed at 12.5 μ eV (0.101 cm $^{-1}$). There could be some drift of the potential in the deuterated compound due to the change of the zero-point energy and/or to some coupling with phonons in the crystal. Nevertheless, even though this approach deserves further refinements, the main features in lithium acetate can be very well understood in terms of tunneling and breather modes in quasi-one-dimensional infinite chains of coupled methyl groups. Therefore, in this case, both the close-contact pair model and the sine-Gordon theory lead to similar agreement with the experiments, even though their physical bases

TABLE VII. Lithium acetate. Soliton and breather modes in the sine-Gordon potential: $V(\theta_j) = \frac{59}{2}(1 - \cos 3\theta_j) + \frac{35}{2}[1 - \cos 3(\theta_{j+1} - \theta_j)]$; V and θ are in cm $^{-1}$ and radian units, respectively. L is the lattice parameter.

CH $_3$ COOLi \cdot 2H $_2$ O	CD $_3$ COOLi \cdot 2D $_2$ O	
5.219	2.609	Rotational constant F (cm $^{-1}$) = $h_2/8\pi_2I_r$ (Ref. 22).
2.183 (2.015)	0.330 (0.101)	Calculated (observed Ref. 22) in-phase tunneling frequencies.
1.743 (1.725)	0.171 (0.101)	Calculated (observed Ref. 22) out-of-plane tunneling frequencies.
37.22	26.32	ω_0 (cm $^{-1}$)
28.67	20.27	ω_c (cm $^{-1}$)
0.59	0.59	d/L : particle width parameter.
181.77	181.77	E_0 (cm $^{-1}$): rest energy of the classical soliton.
116.68	116.68	E_K (cm $^{-1}$): renormalized rest energy of the semiclassical soliton.
179.31	179.31	$E_B(1)$ (cm $^{-1}$): renormalized rest energy of the semiclassical breather.
2.278 (2.281)	1.142 (1.048)	Calculated (observed Ref. 22) $0 \rightarrow 1$ transition for the semiclassical breather traveling in an infinite chain.
1.706 (1.451)	0.856 (—)	Calculated (observed Ref. 22) $0 \rightarrow 1$ transition for the semiclassical breather in a box of size $2L$.
23.82	16.84	ω_B (cm $^{-1}$): frequency of the envelope of the semiclassical breather at rest in the fundamental state.
1.17	1.17	Maximum amplitude (in radian units) of the semiclassical breather envelope.

are quite different. Is this due to fundamental ambiguities of the spectra or are crucial measurements able to discriminate between the two models? Presumably a more thorough analysis of the relative intensities and temperature effects on isotopic mixtures should be necessary. In the case of 4MP, on the other hand, to interpret the data in terms of the close-contact pair model Hamiltonian similar to lithium acetate would require many additional couplings in the Hamiltonian [Eq. (3)]. Presumably, coupling terms with phonons [Eq. (6)] might account for the isotopic dilution effects at low temperature and for the temperature effects for a given isotopic concentration. Further terms should be necessary to account for the influence of the isotopic concentration on the temperature effects. It is not clear whether such a complicated Hamiltonian should be tractable. On the contrary, the sine-Gordon theory provides a comprehensive interpretation of the data with a small number of physically sensible parameters. Once V_0 and V_c have been evaluated from the tunneling frequencies, then the breather dynamics is completely represented. Isotopic and temperature effects are simply related to the cluster size statistics and to a first-order law. Even though this is not enough to prove its physical consistency, this theory certainly deserves and stimulates further investigation in the field of methyl rotational dynamics.

CONCLUSION

Inelastic neutron scattering spectra of isotopic mixtures of 4MP- h_7 and 4MP- d_7 show tunneling and collective motion of the methyl groups at low temperature.

The quantum sine-Gordon theory provides a very compact and elegant tool for interpreting the INS spectra and for describing the peculiar dynamics of methyl torsion in 4MP. It is remarkable that the starting equation depends on two parameters (namely the on-site potential V_0 and the strain potential V_c) that are determined experimentally from the tunneling frequencies. Then the theory yields a breather energy spectrum that deviates by less than 5% from the experimental values. Furthermore, the theory provides a clear understanding of isotopic dilution and temperature effects in terms of breather dynamics in finite boxes. This theory deserves further refinements. Some calculations presented in this work are not free of *ad hoc* parameters like the cluster size cutoff for the breather tunneling, or the activation energy for the breather state mixing in isotopic mixtures. Tentative calculations suggest that 4-methyl-pyridine might not be unique and the sine-Gordon theory provides a completely new standpoint for further investigations in the field of methyl tunneling spectroscopy.

ACKNOWLEDGMENTS

We would like to thank Dr. M. F. Lauté from Laboratoire de Spectrochimie Infrarouge et Raman, (LASIR), Centre National de la Recherche Scientifique (CNRS), Thiais, for her careful preparation of the deuterated samples and Mr. A. Smith for his help in the neutron scattering experiments. We would also like to acknowledge valuable discussions with Dr. N. Le Calvé, Dr. B. Pasquier, and Dr. M. Couzi.

-
- ¹H. D. Rudolph, H. Dreizler, and H. Seiler, *Z. Naturforsch.* **22a**, 1738 (1967).
²J. B. Moffat, *J. Mol. Struct.* **32**, 67 (1976).
³J. Haupt, *Phys. Lett.* **38A**, 389 (1972).
⁴J. Haupt, *Z. Naturforsch.* **28a**, 98 (1973).
⁵B. Alefeld, A. Kollmar, and B. A. Dasannacharya, *J. Chem. Phys.* **63**, 4415 (1975).
⁶W. Press, *Single Particle Rotation in Molecular Crystals*, Vol. 92 of *Springer Tracts in Modern Physics* (Springer-Verlag, Berlin, 1981).
⁷K. J. Abed, S. Clough, C. J. Carlile, B. Rosi, and R. C. Ward, *Chem. Phys. Lett.* **141**, 215 (1987).
⁸N. Le Calvé, D. Cavagnat, and F. Fillaux, *Chem. Phys. Lett.* **146**, 549 (1988).
⁹L. Soulard, F. Fillaux, G. Braathen, N. Le Calvé, and B. Pasquier, *Chem. Phys. Lett.* **125**, 41 (1986).
¹⁰N. Le Calvé, B. Pasquier, G. Braathen, L. Soulard, and F. Fillaux, *J. Phys. C* **19**, 6695 (1986).
¹¹A. Péneau, Thèse de Doctorat d'Etat, Université Paris-Sud, Orsay, 1975.
¹²A. Péneau, M. Gourdji, and L. Guibé, *J. Mol. Struct.* **111**, 227 (1983).
¹³S. G. Biswas, *Ind. J. Phys.* **35**, 261 (1961).
¹⁴U. Ohms, H. Guth, W. Treutmann, H. Dannohl, A. Schweig, and G. Hegar, *J. Chem. Phys.* **83**, 273 (1985).
¹⁵C. J. Carlile, *Nucl. Instrum. Methods* (to be published).
¹⁶C. J. Carlile, B. T. M. Willis, R. M. Ibberson, and F. Fillaux, *Z. Kristallogr.* (in press).
¹⁷C. J. Carlile, S. Clough, A. J. Horsewill, and A. Smith, *Chem. Phys.* **134**, 437 (1989).
¹⁸J. R. Durig, S. M. Craven, and W. C. Harris, *Vibrational Spectra and Structure* (Marcel Dekker, New York, 1972), p. 73.
¹⁹D. R. Herschbach (unpublished).
²⁰S. Clough, A. Heidemann, A. J. Horsewill, and M. N. J. Paley, *Z. Phys. B* **55**, 1 (1984).
²¹A. Heidemann, K. J. Abed, C. J. Barker, and S. Clough, *Z. Phys. B* **66**, 355 (1987).
²²A. Heidemann, H. Friedrich, E. Günther, and W. Häusler, *Z. Phys. B* **76**, 335 (1989).
²³K. D. Moller and H. G. Andresen, *J. Chem. Phys.* **37**, 1800 (1962).
²⁴M. Prager, J. Stanislawski, and W. Häusler, *J. Chem. Phys.* **86**, 2563 (1987).
²⁵D. Cavagnat and M. Pesquer, *J. Phys. Chem.* **90**, 3289 (1986).
²⁶A. Scott, F. Chu, and D. McLaughlin, *Proc. IEEE* **61**, 1443 (1973).
²⁷R. Jackiw, *Rev. Mod. Phys.* **49**, 681 (1977).
²⁸R. F. Dashen, B. Hasslacher, and A. Neveu, *Phys. Rev. D* **11**, 3424 (1975).
²⁹M. J. Rice, A. R. Bishop, J. A. Krumhansl, and S. E. Trullinger, *Phys. Rev. Lett.* **36**, 432 (1976).
³⁰S. E. Trullinger, *Solid State Commun.* **29**, 27 (1979).
³¹E. Stoll, T. Schneider, and A. R. Bishop, *Phys. Rev. Lett.* **42**, 937 (1979).

- ³²J. F. Currie, J. A. Krumhansl, A. R. Bishop, and S. E. Trullinger, *Phys. Rev. B* **22**, 477 (1980).
- ³³M. Altenbokum, U. Kaulfuss, and J. J. M. Verbaarschot, *Phys. Rev. D* **34**, 1840 (1986).
- ³⁴R. D. Carlitz and P. A. Millard, *Phys. Rev. D* **37**, 2269 (1988).

- ³⁵S. Coleman, *Phys. Rev. D* **11**, 2088 (1975).
- ³⁶M. B. Fogel, S. E. Trullinger, A. R. Bishop, and J. A. Krumhansl, *Phys. Rev. B* **15**, 1578 (1977).
- ³⁷J. F. Currie, S. E. Trullinger, A. R. Bishop, and J. A. Krumhansl, *Phys. Rev. B* **15**, 1578 (1977).